Bioelectrochemistry 139 (2021) 107738

Contents lists available at ScienceDirect

Bioelectrochemistry

journal homepage: www.elsevier.com/locate/bioelechem

Nanostructured graphitic carbon nitride based ultrasensing electrochemical biosensor for food toxin detection

Vishakha Nirbhaya, Dipti Chauhan, Raghav Jain, Ramesh Chandra, Suveen Kumar *

Department of Chemistry, University of Delhi, Delhi 110007, India

ARTICLE INFO

Article history:
Received 3 November 2020
Received in revised form 23 December 2020
Accepted 3 January 2021
Available online 12 January 2021

Keywords:
Aflatoxin B1
Food toxin
Graphitic carbon nitride
Electrochemical immunosensor
Thionine

ABSTRACT

We report results of the studies related to the fabrication of thionine functionalized graphitic carbon nitride nanosheets based ultrasensing platform for food toxin (Aflatoxin B1, AfB_1) detection. The synthesis of graphitic carbon nitride nanosheets (g-C_3N_4) was carried out by polycondensation of melamine followed by chemical exfoliation. Further, thionine was used for the functionalization of g-C_3N_4 (Thn/g-C_3N_4) and deposited electrophoretically onto the indium tin oxide (ITO) coated glass electrode. The fabricated Thn/g-C_3N_4/ITO electrode was covalently immobilized by EDC-NHS chemistry with anti-aflatoxin B1 (anti-AfB_1) followed by blocking of non-specific sites using BSA molecules. For structural, morphological, functional and electrochemical properties analysis of synthesized nanomaterials and fabricated electrodes X-ray diffraction, scanning electron microscopy, transmission electron microscopy, Fourier transform infrared spectroscopy, atomic force microscopy and cyclic voltammetry techniques were used. The electrochemical response studies of the fabricated biosensing platform (BSA/anti-AfB_1/Thn/g-C_3N_4/ITO) were carried out towards detection of AfB_1 antigen using cyclic voltammetry technique. The obtained electrochemical results indicate that the fabricated biosensing electrode having ability to detect AfB_1 with lower limit of detection of 0.328 fg mL^{-1}, linear detection range in between 1 fg mL^{-1} to 1 ng mL^{-1}, sensitivity of 4.85 μA log [ng^{-1} mL] cm^{-2} with stability upto 7 weeks.

1. Introduction

Nanomaterials have emerged as efficient immobilization matrices in the fabrication of biosensors owing to their excellent electronic, mechanical, optical, magnetic, and thermal properties. They behave differently from their bulk counterparts due to their high surface area to volume ratio and dominance of quantum effects [1]. Various types of metals and metal-based nanomaterials like oxides [2–4], sulphides [5,6], selenides [7,8], carbides [9,10] etc. have been widely employed in the successful development of biosensors. However, these metal-based nanomaterials are synthesized from expensive and high molecular weight hazardous precursors. Also, many of these metal compounds tend to agglomerate and may lose their dispersion property. This difficulty can be overcome by the use of carbonaceous nanomaterials like graphene and its analogs viz. graphene oxide [11–13], multi-walled carbon nanotubes (MWCNTs) [14,15], carbon nanofibers, porous carbon [16] etc. which possess better dispersing ability and comparatively less harmful precursors. These nanomaterials exhibit excellent electron transfer properties, high mechanical strength, astonishing electrical and thermal conductivity with excellent biocompatibility. Along with these outstanding characteristics, researchers have exploited these materials immensely to fabricate biosensors viz. graphene oxide (GO) coated gold electrode to detect food toxin aflatoxin B1 [17], glassy carbon electrode (GCE) modified MWCNTs, and GO electrode for polyphenol detection [18], ITO coated with MoO_3-reduced graphene oxide (rGO) based platform for breast cancer detection [4], graphene based GCE surface for dopamine detection [19] etc. Significant efforts have also been made to explore novel carbonaceous nanomaterials for biosensing applications. One of the promising candidate emerging from this intent is graphitic carbon nitride (g-C_3N_4) [20]. Graphitic carbon nitride nanomaterials are burgeoning semiconductor polymeric materials with a high N:C ratio (=3/4) with a small amount of hydrogen and structure varying from polymer to graphitic. The name "graphitic" is inherited by graphite, as it has a stacked structure with weak van der Waals forces between layers, also recognized as sp^2-hybridized graphene replaced by nitrogen [21]. This infancy carbonaceous nanomaterial has recently come into consideration owing to a medium bandgap of 2.7 eV. It possesses a porous framework with electron-rich properties, along with basic surface functionalities that help in the facile biofunctionalization of the compound. Nevertheless, its

* Corresponding author
E-mail address: suveendev@gmail.com (S. Kumar).

https://doi.org/10.1016/j.bioelechem.2021.107738
1567-5394/

biocompatibility, physicochemical stability, environment friendly and economic availability align it towards biomedical applications such as therapeutic, diagnostic, imaging, and antimicrobial etc. [22–26]. Ma et al. synthesized protonated ultrathin g-C_3N_4 nanosheets and used to fabricate sensing platform to detect heparin. The protonated g-C_3N_4 interacted electrostatically with negatively charged heparin to produce a fluorescent signal [27]. A highly sensitive g-C_3N_4 based fluorescent biosensing platform was developed by Xiang et al. to detect alkaline phosphatase [28]

For the covalent immobilization of biomolecules onto the fabricated surfaces, linker molecules like 3-aminopropyl triethoxy silane (APTES) and 3-mercaptopropyl triethoxy silane (MPTES) have been used. However, these materials are highly toxic and may have lethal effects on the nervous and respiratory systems. Therefore, recent research interest has emerged in using non-toxic and biocompatible materials for biofunctionalization. Thionine (3,7-diaminophenothiazin-5-ium) has endowed the same characteristics as it is an artificial organic cationic dye and belongs to the class of phenothiazinium. Structurally, it is consisted of a planar molecule and demonstrates a reversible mechanism of transfer of two electrons and two protons. Thionine serves as a mediator and a matrix for enzyme immobilization, possesses good conductivity to transfer electron and high electrochemical signal [29]. It has been extensively reviewed for its potential usefulness in sensor applications. Ou *et al.* developed an immunosensor for CEA detection, in which MWCNTs non-covalently modified with thionine act as redox mediator and GNPs–MWCNTs-THI–CHIT multilayer films on polyelectrolyte modified gold electrode acted as immobilization support [30]. Sun *et al.* employed multifunctional material of thionine–graphene oxide nanosheets (T–GOs) for uric acid (UA) detection and Mendiola *et al.* developed DNA biosensor for the selective detection of mutation in BRCA1 gene using thionine as redox indicator [31].

Aflatoxin, a difuranocoumarin derivative, is one of the extremely toxic secondary metabolites which is synthesized by fungal species like *Aspergillus flavus* and *Aspergillus Parasite* through the polyketide pathway. This primarily contaminates cereal crops including wheat, corn, cotton seeds, walnut, peanut, and tree nuts. The extensive AfB1 exposure occurs globally in hot and humid areas. It affects the body via respiratory, mucous, or cutaneous pathways, and elevates the inflammatory response [32,33]. The International Cancer Research Agency has revealed that AfB1 directly targets the liver tissue, its immunosuppressive properties responsible for hepatocellular carcinoma (HCC, i.e., primary liver cancer), which is the sixth most common cancer worldwide [34]. Therefore, aflatoxins exposure should be minimized. Along with

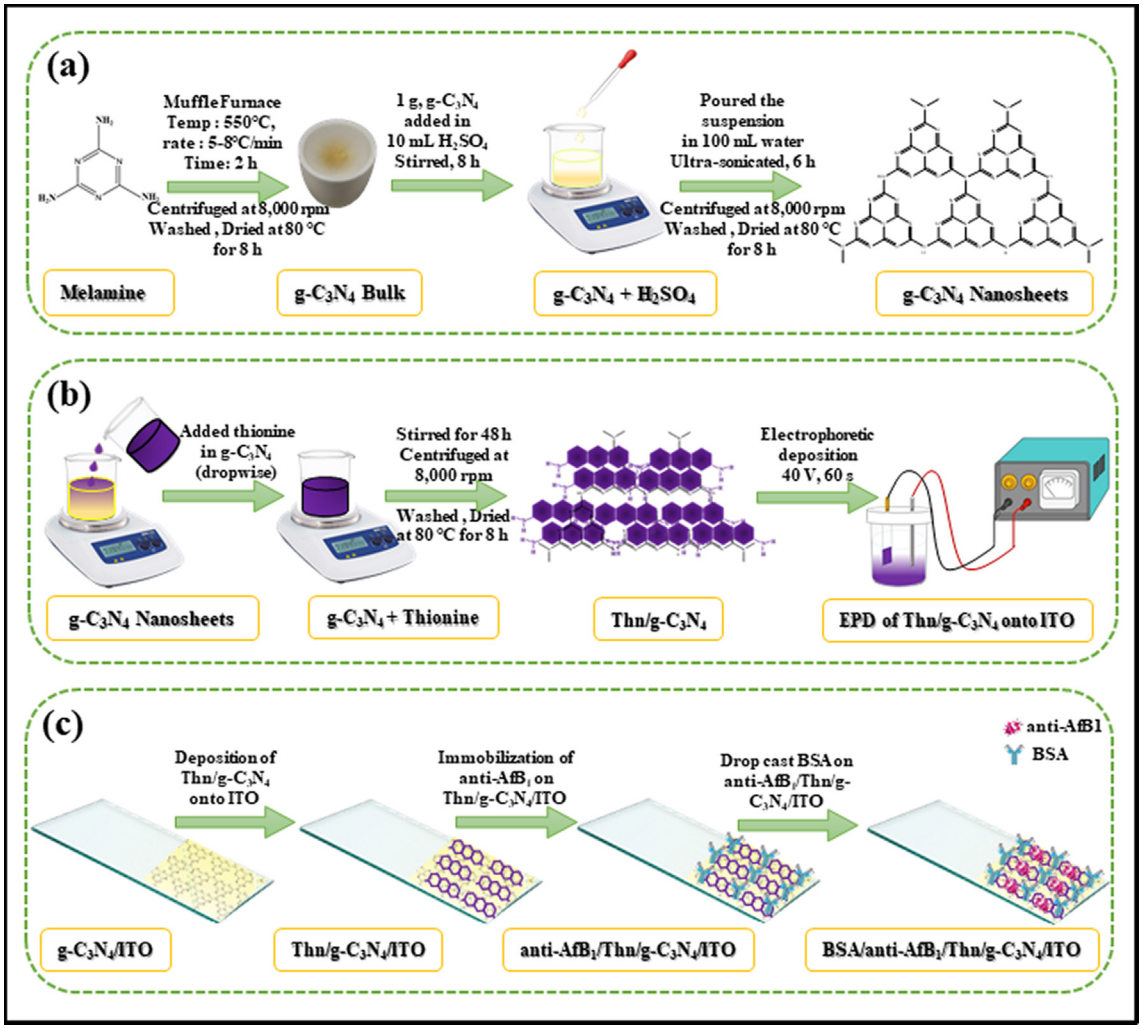

Scheme 1. (a) Synthesis route for the preparation of g-C_3N_4 nanosheets (b) functionalization of g-C_3N_4 nanosheets and electrophoretic deposition of Thn/g-C_3N_4 and, (c) step wise fabrication of biosensing electrode.

this, AfB_1 is not only maleficent to both human and animal health, but also effects food safety and nutrition by limiting access to nutritious food [35]. Conventionally fluorescence spectroscopy, thin layer chromatography (TLC), high performance liquid chromatography (HPLC), liquid chromatography-mass spectroscopy (LCMS), and enzyme linked immunosorbent assay (ELISA) have been used to detect AfB1, but these techniques are time-consuming, commodity-deprived for resource limited area as well as need of qualified practitioners, comprehensive pre-treatment tests and costly equipments. Moreover, to control food safety and human health, an efficient and effective detection technique for AfB_1 urgently needed. Although AfB_1 is a low molecular weight fungal toxin that often leads to weak signals being produced by direct detection, vindicating the production of indirect competitive immunoassay [36]. In this context, biosensor play a vital role in the efficient detection of AfB_1 by minimizing the cost, reducing the analysis time, and applying much simpler techniques. Among different types of biosensors, electrochemical biosensors have recently arisen considerable interest with its high sensitivity, accuracy, rapid detection, and simplicity. Srivastava *et al.* have reported a highly sensitive rGO based biosensing platform for the detection of AfB_1 [37]. Carboxyl functionalized carbon nanotube modified gold electrode was used by Costa *et al.* to fabricate an effective immunosensing platform to detect AfB_1 from corn flour using cyclic voltammetry (CV) and electrochemical impedance spectroscopy (EIS) techniques [38]. The comprehensive review of the enormously developed nanomaterial based biosensing platform hitherto acquiring a lower detection of AfB_1 is still a challenge. To subdue this parameter, nanomaterial owing exquisite biosensing characteristic is the demand of an hour.

In this study, g-C_3N_4 nanosheets were prepared by chemical exfoliation process and further functionalized with thionine (Thn) and biofunctionalized with anti-AfB_1 and bovine serum albumin (BSA) molecules. The biofunctionalized platform was used to develop a biosensor which is competent to detect AfB_1 with ultrasensing lower limit of detection (0.328 fg mL^{-1}), wider linear range (1 fg mL^{-1} to 1 ng mL^{-1}), excellent sensitivity (4.85 μA log [ng^{-1} mL] cm^{-2}), and longer shelf life (7 weeks). To the best of our knowledge, this is the first report towards the development of graphitic carbon nitride based biosensing platform for the detection of food toxin.

2. Materials and methods

2.1. Synthesis of graphitic carbon nitride nanosheets:

The bulk and nanosheets of graphitic carbon nitride were synthesized by polycondensation process. The outline of the synthesis is as follows, 20 g of the melamine was placed in an alumina crucible, covered with the lid, and heated at temperature 550 °C in a Muffle furnace with a heating rate 5 °C–8 °C min^{-1} for 2 h. It was then centrifuged at 8,000 rpm, washed with water and ethanol several times, and dried for 8 h at 80 °C. The bulk form of the graphitic carbon nitride was obtained as a product. For the preparation of graphitic carbon nitride nanosheets, the obtained bulk product g-C_3N_4 (bulk) was further heated in an alumina crucible and covered with a lid at temperature 550 °C in a muffle furnace with a heating rate 10 °C–12 °C min^{-1} for 1 h. To perform chemical exfoliation, 1 g of the obtained product was placed in a beaker and added 10 mL of conc. H_2SO_4 into it and stirred the slurry at room temperature for 8 h. The mixture was poured into a beaker containing 100 mL of de-ionized water and ultrasonicated for 3–4 h. Then centrifuged at 8,000 rpm and washed several times with water and finally with ethanol and dried at 80 °C for 8 h [39] (see Scheme 1a).

2.2. Functionalization of graphitic carbon nitride nanosheets

The 200 mg of g-C_3N_4 and 200 mg of thionine acetate were suspended in 200 mL of DMF, ultrasonicated for 30 min to form suspension and solution respectively. Then thionine solution was added dropwise into 200 mL of g-C_3N_4 suspension and stirred for 48 h at room temperature. The mixture was centrifuged at 12,000 rpm and washed thoroughly with DMF to collect the sediments. The product was dried in an oven at 80 °C overnight and ground using mortar and pestle to form fine powder for further use (see Scheme 1b).

2.3. Electrophoretic deposition of functionalized graphitic carbon nitride nanosheets

The 20 mg of Thn/g-$C_3N_4$was dispersed in 20 mL DMF using ultrasonication for 24 h and a suspension was obtained. 7.0 mL of suspension was taken in a beaker and 300–400 μL of $Mg(NO_3)_2 \cdot 6H_2O$ (1 mg mL^{-1}) was added into it. The classical two electrodes system consisting of an anode ITO coated glass electrode (working electrode) and platinum wire (reference electrode) as a cathode electrode was used for electrophoretic deposition (EPD) technique. An optimized DC potential of 40 V was supplied for the 60 s to form a thin and blackish-blue layer of Thn/g-C_3N_4 on the ITO electrode. The prepared electrodes were washed with deionized water to remove any unbounded materials and stored at room temperature (25 °C) for further use.

2.4. Fabrication of biosensing platform

The covalent amide (—C(O)—NH—) bond formation was accomplished using EDC-NHS coupling chemistry, the carboxylic group present onto the Fc region of the antibody can be covalently immobilized onto an amine residue of Thn/g-C_3N_4/ITO electrode. The optimized concentration ratio of EDC:NHS:antibody was 1:1:2. The outline of the protocol is as follows, 30 μL of anti-AfB1 solution (50 μg mL^{-1} in PBS), 15 μL of EDC (0.4 M), and 15 μL NHS (0.1 M) was placed in an Eppendorf for 30 min at room temperature for the activation of –COOH groups of anti-AfB1. 20 μL of the above formed solution was drop cast uniformly over the Thn/g-C_3N_4/ITO electrode and kept at room temperature for overnight. The obtained anti-AfB1/Thn/g-C_3N_4/ITO electrode was washed with PBS to remove unbound antibody molecules. Further, 20 μL of bovine serum albumin (BSA) was spread over anti-AfB1/Thn/g-C_3N_4/ITO electrode to block the non-specific sites of the electrode and kept it for 2 h at room temperature. After that, the fabricated electrode was washed with PBS solution to remove unbound BSA molecules. After washing, the fabricated BSA/anti-AfB1/Thn/g-C_3N_4/ITO biosensing electrode was stored at 4 °C till further use. The stepwise process used for the fabrication of biosensing platform for AfB_1 detection is shown in Scheme 1c.

3. Results and discussion

3.1. Structural and morphological studies

The X-ray diffraction (XRD) spectra of the synthesized bulk g-C_3N_4 and g-C_3N_4 nanosheets are shown in Fig. 1a, two characteristic peaks were observed for g-C_3N_4 nanosheets which were collective with bulk g-C_3N_4, which signifies that the initial atomic structure of bulk g-C_3N_4 was reserved. Herein, the diffraction peaks attributed to (002) and (100) planes are well indexed in JCPDS No. 87-1526, the intense peak approximately at 27.7° indexed as the (002) plane reflects the stacking of the interlayer of aromatic systems and the weak characteristic peak approximately at 13.0° is

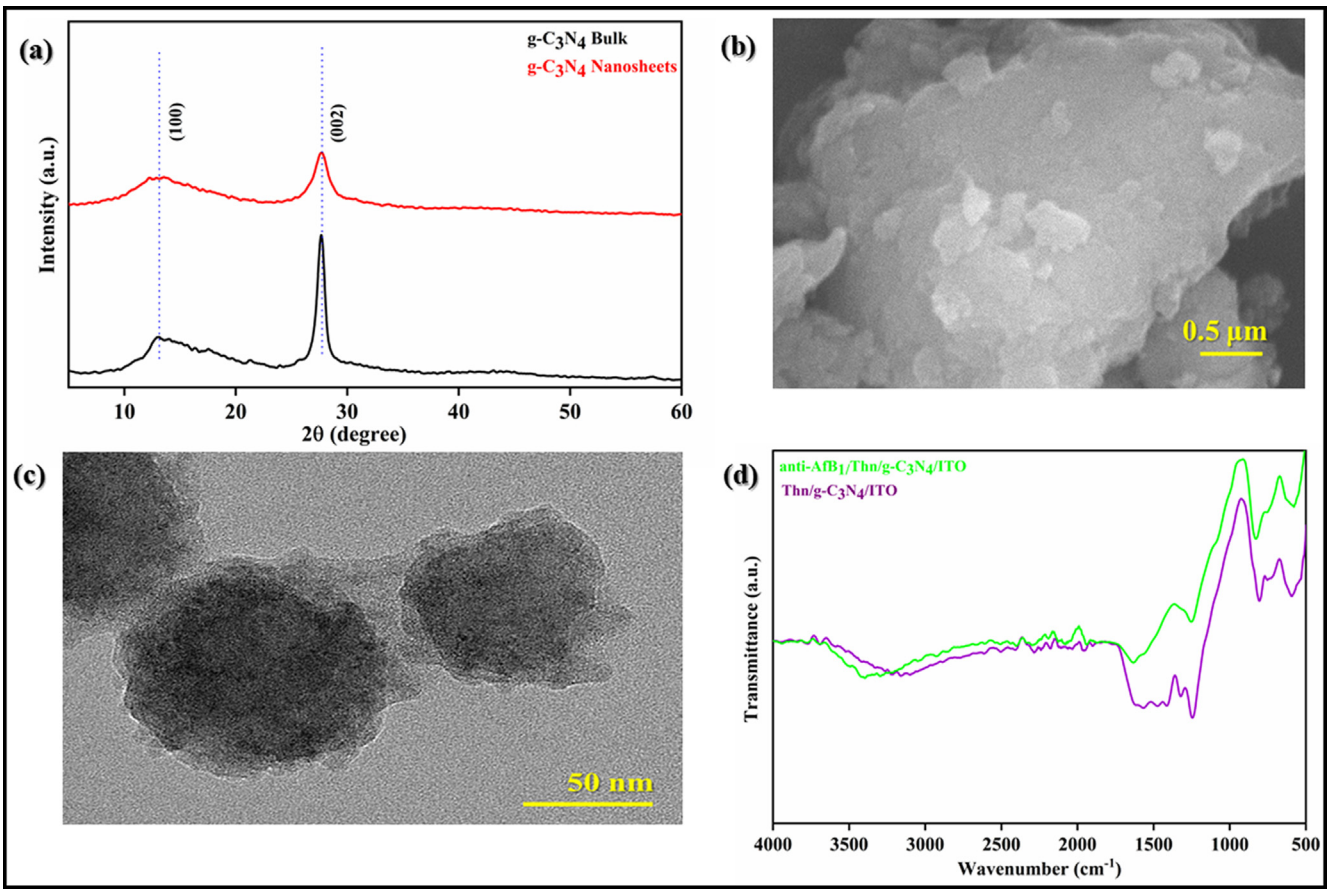

Fig. 1. (a) The XRD pattern of the bulk g-C_3N_4 and g- C_3N_4 nanosheets, (b) SEM image, (c) TEM image of g-C_3N_4 nanosheets and (d) FT-IR spectra of Thn/g-C_3N_4/ITO and anti-AfB_1/Thn/g-C_3N_4/ITO electrodes.

indexed as the (100) plane represents intralayer motif of the heptazine units. The (002) reflection peak shifted from 27.6° to 27.7° for bulk g-C_3N_4 and g-C_3N_4 nanosheets respectively, d-spacing reduced from 0.322 to 0.321 nm corresponding to the decrease in interlayer stacking, and (100) reflection peak at 13.0° shifted to 12.8° from bulk g-C_3N_4 to g-C_3N_4 nanosheets, a d-spacing increase from 0.675 to 0.686 nm which attributed to increase in intralayer distance. The cumulative diffraction intensities of the g-C_3N_4 nanosheets (100) and (002) peaks have become weaker and wider, which was attributed to the reduced thickness of the sheet with short periodicity [40,41]. The peak obtained at 2θ = 27 .7° have a high intensity as compared to 2θ = 13.0° both in bulk and g-C_3N_4 nanosheets, which attributed that the overall growth is along to (002) plane [42].

The morphology of chemically exfoliated g-C_3N_4 nanosheets was studied by scanning electron microscopy (SEM) as well as transmission electron microscopy (TEM) and shown in Fig. 1b and 1c respectively. The SEM image displayed a two dimensional flat layered nanosheet-like structure. Further for a better understanding of g-C_3N_4 nanosheet's morphology, TEM analysis was carried out. TEM image showed that exfoliated g-C_3N_4 are flaky structure with transparent edges, lamellar and planar thin nanosheets, no lattice fringes have appeared which indicates amorphous existence of g-C_3N_4 nanosheets [43].

3.2. Fourier transform infrared spectroscopy (FT-IR) studies

The FT-IR studies were performed to investigate the successful functionalization of synthesized g-C_3N_4 nanosheets with thionine (Fig. S1) along with covalent immobilization of anti-AfB1 onto the electrophoretically fabricated Thn/g-C_3N_4/ITO electrode (Fig. 1d). As shown in Fig. S1, the FT-IR spectra of g-C_3N_4 nanosheets and thionin functionalized g-C_3N_4 nanosheets, the strong and wide peak obtained at 3200 cm^{-1} was correlated to the N-H str as a result of the hydrogenation of sp^2-N. The basic peaks for the stretching and bending modes of N-containing heterocycles were assigned to the band obtained from 1000 cm^{-1} to 1750 cm^{-1} and a peak at 890 cm^{-1}. Furthermore, on elaboration the peaks appeared at 1238 cm^{-1}, 1319 cm^{-1}, 1458 cm^{-1} and 1630 cm^{-1} were correlated to the skeletal vibrations of the heptazine heterocyclic ring (C_6N_7) units and peak at 1410 cm^{-1} as the characteristic peak for the stretching vibration of the s-triazine ring (C_3N_3) units. On comparing the FT-IR spectra of g-C_3N_4 and thionine, no shift but only the intensification of peaks was observed which concluded that the skeletal structure of g-C_3N_4 is intact due to the noncovalent functionalization of g-C_3N_4 nanosheets occurring through π-π stacking and hydrophobic interactions between these two types of conjugated structures. Moreover, g-C_3N_4 nanosheets resemble the structure of GO, π-π stacking might justify the cross-linking of thionine and g-C_3N_4 nanosheets. Fig. 1d shows the FT-IR spectra of Thn/g-C_3N_4/ITO and anti-AfB1/Thn/g-C_3N_4/ITO electrodes. In the spectra of anti-AfB1/Thn/g-C_3N_4/ITO electrode, a wide band was obtained in between 3200 and 3450 cm^{-1} shifted to a higher frequency than Thn/g-C_3N_4/ITO electrode 3100–3300 cm^{-1}, which ascribed the N-H str due to the transformation of amide group from amine group. The peaks obtained at 1635 cm^{-1} and ~1251 cm^{-1} are associated with C═O and C—N stretching vibration respectively which further confirm the formation of amide bond [41,44].

3.3. Topological studies

The topology of the fabricated electrodes using atomic force microscopy (AFM) technique was investigated to confirm the step wise fabrication of biosensing platform and obtained results are as shown in Fig. 2. The AFM image of Thn/g-C_3N_4/ITO electrode (Fig. 2a and 2b) illustrated uniformly placed spines like morphology with an average roughness of ≈6.7 nm, which suggests that functionalized g-C_3N_4 uniformly deposited onto the ITO electrode. Subsequently, the immobilization of anti-AfB_1 over Thn/g-C_3N_4/ITO electrode (Fig. 2c and 2d), the surface roughness increased to ≈11.0 nm. The presence of the globular structure of the antibody confirms the effective immobilization of anti-AfB_1 on the Thn/g-C_3N_4/ITO electrode because of this morphological transition. After BSA molecules are immobilized on the anti-AfB_1/Thn/g-C_3N_4/ITO electrode, (Fig. 2e and 2f), the average roughness increased to ≈82.6 nm as a result of gigantic size of BSA molecules [7], which confirmed the presence of BSA molecules. The AFM studies also revealed that at each fabrication step, as a view of topology Z-height increased from 40 nm to 200 nm, which signified successful attachment of antibody and BSA molecules onto Thn/g-C_3N_4/ITO electrode.

3.4. Electrochemical characterization

To study the electrochemical characterization of all the fabricated electrodes, CV technique was used, which holds the capability to rapidly observe the redox behaviour of an organic/inorganic chemical or a biomolecule over a wide range of potential. A three electrodes system i.e., ITO coated glass substrate as working electrode (WE), platinum as auxiliary/counter electrode (CE) and Ag/AgCl as reference electrode (RE) was used to study the effect of ferri/ferrocyanide {$[Fe(CN)_6]^{3-/4-}$}. Firstly the CV study was carried out in 0.2 M phosphate buffer saline (PBS) solution and then in PBS (0.2 M) containing $[Fe(CN)_6]^{3-/4-}$ (5 mM) using ITO electrode at a scan rate of 50 mV s^{-1} and the obtained results are shown in

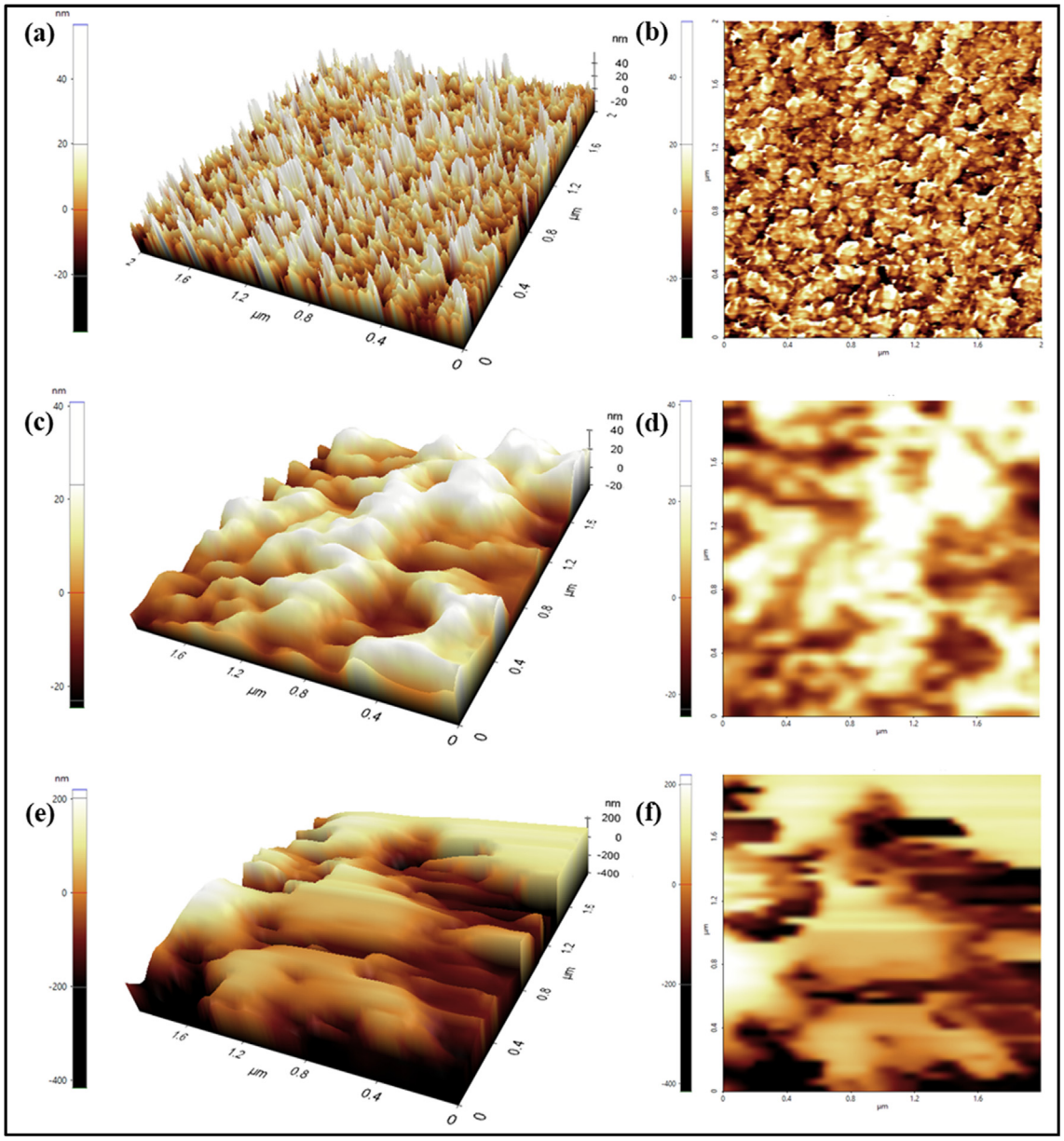

Fig. 2. 2D and 3D AFM images of (a, b) Thn/g-C_3N_4/ITO, (c, d) anti- AfB_1/Thn/g-C_3N_4/ITO and (e, f) BSA/anti-AfB_1/Thn/g-C_3N_4/ITO electrodes.

Fig. S2. The PBS without ferri/ferrocyanide, showed the poor signal, thus an electroactive species, i.e., $[Fe(CN)_6]^{3-/4-}$ was employed to enhance the oxidation and reduction peak current by the virtue of its facile electron transfer and electronic amplification. So, for further electrochemical studies, PBS (0.2 M) containing $[Fe(CN)_6]^{3-/4-}$ (5 mM) solution was used. The pH studies were then conducted to investigate the favourable pH of PBS buffer for the fabricated BSA/anti-AfB_1/Thn/g-C_3N_4/ITO electrode. For this study, at a scan rate of 50 mV s^{-1}, PBS containing $[Fe(CN)_6]^{3-/4-}$ was used and attained electrochemical response of BSA/anti-AfB_1/Thn/g-C_3N_4/ITO electrode as a function of pH (5.7–8.0) and the obtained results are shown in Fig. S3. The obtained results disclose that the charge present onto the proteinaceous biomolecules depend directly on the pH of buffer solution in which they are immersed and ultimately affect the electrochemical response [45]. Further, a graph was plotted for peak current (oxidation) as a function of pH and observed that at pH 7.0, maximum anodic current was obtained (Inset of Fig. S3), which suggested that at neutral pH this proteinaceous biomolecule (i.e., antibody) is present in its native form, show high stability and activity. However, in acidic or basic pH range these substances fetched to denatured because of the involvement of H^+ or OH^- ions on the amino acid of the antibodies [46]. It is a trivial thought that at pI (Isoelectric point) biomolecules might have shown a high current response also, although moderate pI adversely affects the electrochemical response [45], taking this into consideration further electrochemical studies have been investigated using PBS at pH 7.0.

To examine the effect of scan rate, the electrochemical response was studied on the Thn/g-C_3N_4/ITO and BSA/anti-AfB_1/Thn/g-C_3N_4/ITO electrodes as a function of scan rate in the range 10–100 mV s^{-1} and the obtained results are shown in Fig. S4 and 3 (i) respectively. We ascertained that both the anodic and the cathodic peak current vary linearly with the square root of the scan rate, which implied that the electrochemical reaction is a mechanism of diffusion regulation [2]. The inset (a) of Fig. S4 and 3 (i)shows the variation of anodic (I_{Pa}) and cathodic (I_{Pc}) peak current vs square root of scan rate and follow Eqs. (1)–(4):

$$I_{Pa(Thn/g\text{-}C3N4/ITO)} = [0.035 \pm 0.001\ mA \times (\text{scan rate } [mV/s])^{1/2}] + 0.074 \pm 0.008\ mA, \quad R^2 = 0.99 \tag{1}$$

$$I_{Pc(Thn/g\text{-}C3N4/ITO)} = [-0.025 \pm 0.001\ mA \times (\text{scan rate } [mV/s])^{1/2}] - 0.104 \pm 0.009\ mA, \quad R^2 = 0.97 \tag{2}$$

$$I_{Pa(BSA/anti\text{-}AfB1/Thn/g\text{-}C3N4/ITO)} = [0.325 \pm 0.001\ mA \times (\text{scan rate } [mV/s])^{1/2}] - 0.147 \pm 0.024\ mA, \quad R^2 = 0.98 \tag{3}$$

$$I_{Pc(BSA/anti\text{-}AfB1/Thn/g\text{-}C3N4/ITO)} = [-0.2438 \pm 0.0105\ mA \times (\text{scan rate } [mV/s])^{1/2}] - 0.077 \pm 0.0177\ mA, \quad R^2 = 0.98 \tag{4}$$

Moreover, the peak-to-peak separation was shifted with increasing scan rate [inset (b) of Figs. S4 and 3 (i)] which concluded that the procedure is electrochemically quasi-reversible [46,47].

The difference in the peak potentials of cathodic (Epc) and anodic (Epa) (ΔEp = Epa- Epc) as a function of the square root of scan rate for Thn/g-C_3N_4/ITO and BSA/anti-AfB_1/Thn/g-C_3N_4/ITO electrodes demonstrated a linear relationship given by the Eqs. (5) and (6). It suggested a facile transfer of electrons from medium to the electrode.

$$\Delta Ep_{(Thn/g\text{-}C3N4/ITO)} = \left[0.040 \pm 0.0016\ V \times (\text{scan rate}[mV/s])^{1/2}\right] + 0.387 \pm 0.012V, \quad R^2 = 0.98 \tag{5}$$

$$\Delta Ep_{(BSA/anti\text{-}AfB1/Thn/g\text{-}C3N4/ITO)} = \left[0.221 \pm 0.005\ V \times (\text{scan rate}[mV/s])^{1/2}\right] + 0.033 \pm 0.008\ V, \quad R^2 = 0.99 \tag{6}$$

The Randles-Sevcik equation was used to determine the diffusion coefficient of the redox species $[Fe(CN)_6]^{3-/4-}$ Eq. (7)

$$I_p = \left(2.69 \times 10^5\right) n^{\frac{3}{2}} A D^{1/2} C \upsilon^{1/2} \tag{7}$$

where Ip is peak current of the electrode, n is electron stoichiometry, A is the active surface area of electrode (0.25 cm^2), D is diffusion coefficient (cm^2 s^{-1}), C is the concentration of the electroactive species (5 mM), and υ is scan rate (50 mVs^{-1}). The value of the diffusion coefficient has been estimated as 2.67 × 10^{-5} cm^2 s^{-1}, which is higher with respect to the previously reported carboxylated MWCNTs based biosensor (3.79 × 10^{-7} cm^2 s^{-1}) [48] for AfB_1 detection. Therefore, diffusion coefficient depends on the surface area of the working electrode and on the concentration of electro-active species. Also, this signifies that the BSA/anti-AfB_1/Thn/g-C_3N_4/ITO electrode shows faster electron transfer kinetics compared with that of MWCNTs resulting in superior analytical efficiency of this biosensor [48]. The surface concentration of the electrode was estimated using the Brown-Anson model as given in Eq. (8):

$$I_p = n^2 F^2 \gamma A \upsilon (4RT)^{-1} \tag{8}$$

where Ip denotes the peak current, A is the electrode surface area, υ is the scan rate (V s^{-1}), γ is the surface concentration of the absorbed electro-active species, F is the Faraday constant (96485 C mol^{-1}), R is the gas constant (8.314 J mol^{-1} K^{-1}) and T is room temperature (25 °C or 298 K). The surface concentration of BSA/anti-AfB_1/Thn/g-C_3N_4/ITO is estimated to be as 3.25 × 10^{-5} mol cm^{-2}, which indicates that the fabricated electrode can be used for the biosensing application.

The electrochemical studies were performed with 0.2 M PBS of pH = 7 (containing 5 mM $[Fe(CN)_6]^{3-/4-}$) at a scan rate of 50 mV s^{-1} for each step in the fabrication of immunoelectrode and obtained results are shown in Fig. 3 (ii) for (a) ITO, (b) g-C_3N_4/ITO, (c) Thn/g-C_3N_4/ITO, (d) anti-AfB_1/Thn/g-C_3N_4/ITO, and (e) BSA/anti-AfB_1/Thn/g-C_3N_4/ITO electrodes. The magnitude of current obtained for the g-C_3N_4/ITO electrode (0.417 mA) was found to be comparable to the bare ITO electrode (0.427), but the difference is slightly large for Thn/g-C_3N_4/ITO (0.260 mA). The potential was moved marginally to the negative potential, which suggested that deposited layer hindered electron transfer between redox active species and g-C_3N_4/ITO or Thn/g-C_3N_4/ITO electrode surface, which may be difficult to reduce or oxidise. Moreover, after the immobilization of anti-AfB_1 onto Thn/g-C_3N_4/ITO electrode, the peak current drastically increased to 0.482 mA. This is due to the presence of non-binding sites i.e., free NH_3^+ groups onto the anti-AfB_1/Thn/g-C_3N_4/ITO electrode, which subsequently increase electron transfer between anti-AfB_1/Thn/g-C_3N_4/ITO and Thn/g-C_3N_4/ITO electrodes [2,7]. Furthermore, peak current for BSA/anti-AfB_1/Thn/g-C_3N_4/ITO immunoelectrode lowers to 0.383 mA, because of the blocking of non-specific active sites by BSA molecules present at the surface of the biosensing electrode and the movement of electrons between the solution and the surface of the electrode was impeded [46].

3.5. Electrochemical response studies

Before the electrochemical response studies of fabricated biosensing electrode, we conducted the incubation time study (Fig. S5) to determine the incubation time required for the interaction of AfB1 antigen with BSA/anti-AfB1/Thn/g-C_3N_4/ITO immunoelectrode. The process was carried out at a consistent interval of

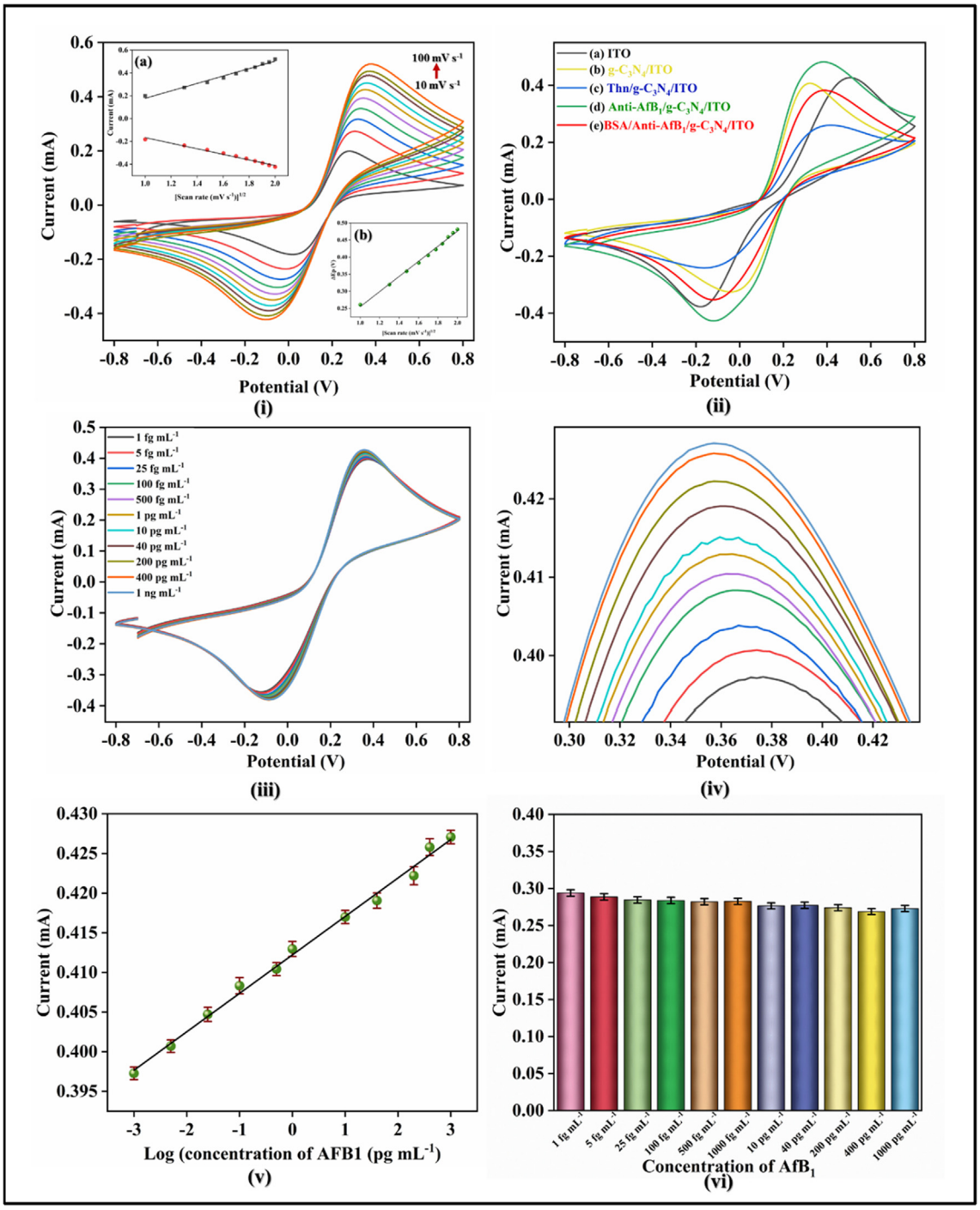

Fig. 3. Scan rate study of (i) BSA/anti-AfB_1/Thn/g-C_3N_4/ITO electrode in between 10 and 100 mVs^{-1}, Inset (a) magnitude of anodic and cathodic peak current as a function of square root of scan rate scan rate (mVs^{-1}) and inset (b) difference of oxidation and reduction peak potential (ΔEp = Epa-Epc) as a function of square root of scan rate ($mV\ s^{-1}$), (ii) The CV of (a) ITO (b) g-C_3N_4/ITO (c) Thn/g-C_3N_4/ITO (d) anti-AfB_1/Thn/g-C_3N_4/ITO and (e) BSA/anti-AfB_1/Thn/g-C_3N_4/ITO electrodes, (iii) Electrochemical response study of BSA/anti-AfB_1/Thn/g-C_3N_4/ITO biosensing electrode as a function of different concentration of AfB1 (1 fg $mL^{-1}$to 1 ng mL^{-1}), (iv) magnified view of oxidation peak current, (v) response current curve as a function of [Log (concentration of AfB1 (ng mL^{-1})] and (vi) control studies of BSA/anti-AfB_1/Thn/g-C_3N_4/ITO immunoelectrode as a function of AfB1 antigen concentration (1 fg mL^{-1} to 1 ng mL^{-1}).

2 min and up to 32 min, by observing the obtained results we chose 15 min as optimum time for the sufficient interaction between AfB1 antigen with BSA/anti-AfB_1/Thn/g-C_3N_4/ITO electrode. Therefore, before each electrochemical measurement, we provided 15 min of incubation time for further electrochemical studies.

The electrochemical response studies of BSA/anti-AfB_1/Thn/g-C_3N_4/ITO biosensing electrode was carried out as a function of AfB_1 antigen concentration (1 fg mL^{-1} to 1 ng mL^{-1}), in PBS (0.2 M) containing $[Fe(CN)_6]^{3-/4-}$ (5 mM) ions at the scan rate of 50 mV s^{-1} and potential ranging from −0.8 V to 0.8 V [Fig. 3 (iii) and 3 (iv)]. The electrochemical response of anodic peak current was observed to increase gradually on increasing the analyte concentration from 1 fg mL^{-1} to 1 ng mL^{-1}, and a linear plot was obtained for peak current vs Log [concentration of AfB_1 (pg mL^{-1})] with a regression coefficient of 0.99 and follows the Eq. (9):

$$\mathrm{Ip} = \left[4.848\mathrm{E}\text{-}6 \pm 1.171\mathrm{E}\text{-}7\ \left(\mathrm{mA\ mL\ pg}^{-1}\right)\right] \times \mathrm{Log}\left[\text{concentration of } \mathrm{AfB_1}\left(\mathrm{pg\ mL}^{-1}\right)\right] + [4.122E-4 \pm 2.304\mathrm{E}-7],\ R^2 = 0.99$$

This concluded that the anodic peak current amplified proportionally with AfB_1 concentration, as a virtue of immunocomplex formation between antigen AfB_1 and anti-AfB_1 antibody specifically on the surface of BSA/anti-AfB_1/Thn/g-C_3N_4/ITO biosensing electrode, provided additional electroactive locations for unstrained electron transfer at the surface of electrode and results to electron transfer layer formation and change in conformational structure [37,49]. For the fabricated BSA/anti-AfB_1/Thn/g-C_3N_4/ITO biosensing electrode sensitivity was estimated to be 4.85 μA log [mL ng $^{-1}$] cm^{-2} using slope of calibration curve (Fig. 3 (v)).

Using the Eq. (10), the LOD is determined to be 0.328 fg mL^{-1}:

$$\mathrm{LOD} = 3 \times \frac{SD}{Slope}$$

$$= 3 \times SD / \frac{dy}{dx}$$

$$= 3 \times SD / \left[\frac{dy}{dlnx} \times \frac{dlnx}{dx}\right]$$

$$= 3 \times SD / \left[\frac{dy}{2.303 dlogx} \times \frac{1}{x}\right]$$

$$= 3 \times SD \times (2.303 \times x) / \left[\frac{dy}{dlogx}\right]$$

$$= 3 \times SD \times (2.303 \times x)/\text{Slope of Semi log plot} \quad (10)$$

where x is the lowest measured concentration or the limit of quantification, SD is the standard deviation of intercept [50].

Moreover, the proposed biosensing platform offered an inclusive linear range of detection from 1 fg mL^{-1} to 1 ng mL^{-1}, with a limit of detection 0.328 fg mL^{-1}. The accomplished linearity and lower limit of detection of biosensing platform have been improvised than previously reported nanomaterial based biosensors as compared to Au@rGO nanocomposite [51], chitosan-AuNPs nanocomposite [52], graphene quantum dots and gold nanoparticles (GQD-AuNP) nanocomposite [49], screen-printed electrode based electrochemical immunosensor [36] etc. The acquired efficient biosensing parameters by fabricated platform may be due to graphitic carbon nitride nanosheets as the immobilization matrix. It possesses large specific surface which can accommodate ample number of biomolecules [53]. Furthermore, the presence of electron rich covalent framework, the ultrathin structure of g-C_3N_4 nanosheets is accountable for fast electron carrier transport [54]. Therefore, ultrathin g-C_3N_4 nanosheets might produce enhanced electrochemical response at very low concentration of biomolecules (i.e., ultrasensing limit of detection 0.328 fg mL^{-1}, linear detection range 1 fg mL^{-1}to 1 ng mL^{-1}), it has enhanced the efficiency of charge transport which led to highly sensitive detection of AfB_1. The electrochemical sensing parameters of the fabricated BSA/anti-AfB_1/Thn/g-C_3N_4/ITO electrode based biosensor for AfB_1 detection has been compared with those reported in the literature in Table 1.

3.6. Control and interferent studies

The control experiment was conducted to examine the cross-reactivity of Thn/g-C_3N_4/ITO electrode with the varying concentration of the AfB1 antigen and the obtained results are shown in Fig. 3 (iv). All the parameters were kept similar as the electrochemical response studies for BSA/anti-AfB_1/Thn/g-C_3N_4/ITO electrode except the immobilization of anti-AfB_1. Significantly no substantial change was observed in the magnitude of the peak current of the Thn/g-C_3N_4/ITO electrode with increasing concentration of the AfB_1 antigen, which demonstrated that no interaction occurred between AfB_1 antigen and Thn/g-C_3N_4/ITO electrode. Thus, the change in current in response studies is primarily due to the interaction between antigen and antibody. The interferent studies were explored on BSA/anti-AfB_1/Thn/g-C_3N_4/ITO immunoelectrode using several analytes present in the human serum i.e., glucose, urea, alanine, uric acid, sodium chloride and ascorbic acid. On subsequent addition of analytes, no significant change in anodic current was obtained whereas the current response decreased rapidly after adding AfB_1 antigen due to antibody-antigen interaction (Fig. S6). Moreover, the average %RSD (percentage relative standard deviation) value was estimated to be ~3.98% which is within acceptable limit. All these parameters favour the selective detection of AfB_1 antigen using the fabricated BSA/anti-AfB_1/Thn/g-C_3N_4/ITO biosensing electrode.

3.7. Reproducibility and shelf life studies

The reproducibility studies were carried out by observing the anodic current response of five distinct working electrodes (BSA/anti-AfB_1/Thn/g-C_3N_4/ITO) under similar experimental conditions. A slight variation in current was observed (Fig. S7) and the %RSD for fabricated immunoelectrodes was estimated to be ~5.07%, which is under acceptable range, indicating fair precision and capability to give reproducible results. The BSA/anti-AfB_1/Thn/g-C_3N_4/ITO biosensing electrode's shelf life studies were investigated by monitoring of changes in magnitude of peak current obtained through CV technique using standard solution AfB_1 (500 fg mL^{-1}) in PBS (5 mM $[Fe(CN)_6]^{3-/4-}$) over one-week interval (Fig. S8). The obtained results indicate that the fabricated immunoelectrode is stable upto 7 weeks, after that the peak current start decreasing with respect to the peak current of reference biosensing electrode.

4. Conclusions

In the present work, graphitic carbon nitride nanosheets based an efficient electrochemical biosensor is developed for detection of food toxin AfB_1. Graphitic carbon nitride nanosheets were synthesized through polycondensation reaction and further functionalized by non-toxic thionin (phenothiazine) redox dye. Further, anti-AfB_1 covalently immobilized onto the Thn/g-C_3N_4/ITO electrode using EDC-NHS cross linkers and BSA was used for blocking of non-specific binding sites. The fabricated electrochemical biosensor has ability to detect AfB1 food toxin with ultrasensing lower limit of detection 0.328 fg mL^{-1} in wide concentration range of AfB1 from 1 fg mL^{-1} to 1 ng mL^{-1} and sensitivity of 4.85 μA log [ng^{-1} mL] cm^{-2}. Along with this, the developed biosensor also showed high reproducibility with shelf life of 7 weeks. This analogous approach can also be utilized to identify other mycotoxins like ochratoxin, citrinine, etc. using their respective antibodies. Along with this, graphitic carbon nitride nanosheets opens a new window for use in development of biosensors for various disease detection.

CRediT authorship contribution statement

Vishakha Nirbhaya: Formal analysis, Writing - original draft. **Dipti Chauhan:** Formal analysis. **Raghav Jain:** Formal analysis. **Ramesh Chandra:** Writing - review & editing. **Suveen Kumar:** Methodology, Supervision, Writing - review & editing.

Table 1
A comparative analysis of biosensing parameters of previously fabricated biosensors for AfB_1 detection with present work.

S. No.	Technique	Materials used	Linear range	LOD	Sensitivity	Shelf life	Ref.
1	CV, EIS, AFM	SPEs	50 fg mL^{-1} to 5 ng mL^{-1}	50 fg mL^{-1}	18 μA ng^{-1} mL	–	[36]
2	DPV	PTH/Au/GCE	0.6–2.4 ng mL^{-1}	0.07 ng mL^{-1}	1.23 × 10^{-6}A ng^{-1} mL	–	[55]
3	CV, DPV	C-AuNP/ MBA/Au	10 ng dL^{-1} to 100 ng dL^{-1}	17.90 ng dL^{-1}	0.45 μA ng^{-1} dL (CV) 4.4 μA ng^{-1}dL (DPV)	–	[56]
4	CV	PEDOT/AuNPs/ITO	1 to 25 ng mL^{-1}	0.004 ng mL^{-1}	3.72 μA ng^{-1} mL	–	[57]
5	CV, DPV	Fc/MWCNT/CS/SPE	1 × 10^{-3} to 2 × 10^{4} ng mL^{-1}	0.159 pg mL^{-1}	–	–	[58]
6	CV	CS-AuNPs/gold microelectrode	0.2 to 2 ng mL^{-1} 2 to 30 ng mL^{-1}	0.12 ng mL^{-1}	72.3 μA ng^{-1} mL 0.06 μA ng^{-1} mL	–	[52]
7	CV	c-MWCNTs/ITO	0.25 to 1.375 ng mL^{-1}	0.08 ng mL^{-1}	95.2 μA ng^{-1} mL cm^{-2}	45 days	[48]
8	CV	GQDs-AuNPs/ITO	0.1 to 3.0 ng mL^{-1}	0.008 ng mL^{-1}	382 μA ng^{-1} mL cm^{-2}	–	[49]
9	**CV**	**Thn/g-C_3N_4/ITO**	**1 fg $mL^{-1}$to 1 ng mL^{-1}**	**0.328 fg mL^{-1}**	**4.85 μA log [ng^{-1} mL] cm^{-2}**	**7 weeks**	**Present work**

Declaration of Competing Interest

The authors declare that they have no known competing financial interests or personal relationships that could have appeared to influence the work reported in this paper.

Acknowledgement

We are thankful to the Vice Chancellor of the University of Delhi for providing the requisite facilities and infrastructure. VN and DC have recognised the Council of Scientific and Industrial Research (09/045(1662)/2019-EMR-I) and UGC fellowship (191620082661) for financial support, respectively. SK acknowledge DST INSPIRE faculty scheme (DST/INSPIRE/04/2017/001336) for financial support. The authors acknowledge the access to XRD, FT-IR, SEM and AFM provided by the University Science Instrumentation Centre (USIC) and Central Experimental Facilities. Authors also thankful to SAIF, AIIMS-Delhi for providing TEM facility.

Appendix A. Supplementary material

Supplementary data to this article can be found online at https://doi.org/10.1016/j.bioelechem.2021.107738.

References

[1] T. Daniel, T.N. Manjubaashini, S. Thomas, H.J. Maria, Engineering Materials, n.d. http://www.springer.com/series/4288.
[2] S. Kumar, S. Kumar, S. Tiwari, S. Srivastava, M. Srivastava, B.K. Yadav, S. Kumar, T.T. Tran, A.K. Dewan, A. Mulchandani, J.G. Sharma, S. Maji, B.D. Malhotra, Biofunctionalized nanostructured zirconia for biomedical application: a smart approach for oral cancer detection, Adv. Sci. 2 (2015), https://doi.org/10.1002/advs.201500048.
[3] S. Kumar, M. Umar, A. Saifi, S. Kumar, S. Augustine, S. Srivastava, B.D. Malhotra, Electrochemical paper based cancer biosensor using iron oxide nanoparticles decorated PEDOT:PSS, Anal. Chim. Acta 1056 (2019) 135–145, https://doi.org/10.1016/j.aca.2018.12.053.
[4] S. Augustine, P. Kumar, B.D. Malhotra, Amine-functionalized MoO3@RGO nanohybrid-based biosensor for breast cancer detection, ACS Appl. Bio Mater. 2 (2019) 5366–5378, https://doi.org/10.1021/acsabm.9b00659.
[5] X. Li, Y. Li, Q. Qiu, Q. Wen, Q. Zhang, W. Yang, L. Yuwen, L. Weng, L. Wang, Efficient biofunctionalization of MoS 2 nanosheets with peptides as intracellular fluorescent biosensor for sensitive detection of caspase-3 activity, J. Colloid Interface Sci. 543 (2019) 96–105, https://doi.org/10.1016/j.jcis.2019.02.011.
[6] H. Dai, D. Chen, P. Cao, Y. Li, N. Wang, S. Sun, T. Chen, H. Ma, M. Lin, Molybdenum sulfide/nitrogen-doped carbon nanowire-based electrochemical sensor for hydrogen peroxide in living cells, Sens. Actuators, B 276 (2018) 65–71, https://doi.org/10.1016/j.snb.2018.08.081.
[7] D. Chauhan, V. Pooja, C.M. Nirbhaya, R. Srivastava, S.K. Chandra, Nanostructured transition metal chalcogenide embedded on reduced graphene oxide based highly efficient biosensor for cardiovascular disease detection, Microchem. J. 155 (2020), https://doi.org/10.1016/j.microc.2020.104697.
[8] C. Chaudhary, S. Kumar, R. Chandra, Monophasic molybdenum selenide-reduced graphene oxide nanocomposite sheets based immunosensing platform for ultrasensitive serotonin detection, Microchem. J. 159 (2020), https://doi.org/10.1016/j.microc.2020.105344.
[9] L. Zhou, X. Zhang, L. Ma, J. Gao, Y. Jiang, Acetylcholinesterase/chitosan-transition metal carbides nanocomposites-based biosensor for the organophosphate pesticides detection, Biochem. Eng. J. 128 (2017) 243–249, https://doi.org/10.1016/j.bej.2017.10.008.
[10] Y. Jiang, X. Zhang, L. Pei, S. Yue, L. Ma, L. Zhou, Z. Huang, Y. He, J. Gao, Silver nanoparticles modified two-dimensional transition metal carbides as nanocarriers to fabricate acetycholinesterase-based electrochemical biosensor, Chem. Eng. J. 339 (2018) 547–556, https://doi.org/10.1016/j.cej.2018.01.111.
[11] S. Kumar, S. Ashish, S. Kumar, S. Augustine, B.K. Yadav, R.P. Yadav, A.K. Chauhan, B.D. Dewan, Malhotra, Effect of Brownian motion on reduced agglomeration of nanostructured metal oxide towards development of efficient cancer biosensor, Biosens. Bioelectron. 102 (2018) 247–255, https://doi.org/10.1016/j.bios.2017.11.004.
[12] D. Sandil, S. Srivastava, B.D. Malhotra, S.C. Sharma, N.K. Puri, Biofunctionalized tungsten trioxide-reduced graphene oxide nanocomposites for sensitive electrochemical immunosensing of cardiac biomarker, J. Alloy. Compd. 763 (2018) 102–110, https://doi.org/10.1016/j.jallcom.2018.04.293.
[13] S. Zhang, N. Huang, Q. Lu, M. Liu, H. Li, Y. Zhang, S. Yao, A double signal electrochemical human immunoglobulin G immunosensor based on gold nanoparticles-polydopamine functionalized reduced graphene oxide as a sensor platform and AgNPs/carbon nanocomposite as signal probe and catalytic substrate, Biosens. Bioelectron. 77 (2016) 1078–1085, https://doi.org/10.1016/j.bios.2015.10.089.
[14] F. Mo, J. Xie, T. Wu, M. Liu, Y. Zhang, S. Yao, A sensitive electrochemical sensor for bisphenol A on the basis of the AuPd incorporated carboxylic multi-walled carbon nanotubes, Food Chem. 292 (2019) 253–259, https://doi.org/10.1016/j.foodchem.2019.04.034.
[15] S. Zhang, R. Li, X. Liu, L. Yang, Q. Lu, M. Liu, H. Li, Y. Zhang, S. Yao, A novel multiple signal amplifying immunosensor based on the strategy of in situ-produced electroactive substance by ALP and carbon-based Ag-Au bimetallic as the catalyst and signal enhancer, Biosens. Bioelectron. 92 (2017) 457–464, https://doi.org/10.1016/j.bios.2016.10.080.
[16] K. Mondal, M.A. Ali, C. Singh, G. Sumana, B.D. Malhotra, A. Sharma, Highly sensitive porous carbon and metal/carbon conducting nanofiber based enzymatic biosensors for triglyceride detection, Sens. Actuators, B 246 (2017) 202–214, https://doi.org/10.1016/j.snb.2017.02.050.
[17] S. Srivastava, M.A. Ali, S. Umrao, U.K. Parashar, A. Srivastava, G. Sumana, B.D. Malhotra, S.S. Pandey, S. Hayase, Graphene oxide-based biosensor for food toxin detection, Appl. Biochem. Biotechnol. 174 (2014) 960–970, https://doi.org/10.1007/s12010-014-0965-4.
[18] Y. Vlamidis, I. Gualandi, D. Tonelli, Amperometric biosensors based on reduced GO and MWCNTs composite for polyphenols detection in fruit juices, J. Electroanal. Chem. 799 (2017) 285–292, https://doi.org/10.1016/j.jelechem.2017.06.012.
[19] Y.R. Kim, S. Bong, Y.J. Kang, Y. Yang, R.K. Mahajan, J.S. Kim, H. Kim, Electrochemical detection of dopamine in the presence of ascorbic acid using graphene modified electrodes, Biosens. Bioelectron. 25 (2010) 2366–2369, https://doi.org/10.1016/j.bios.2010.02.031.
[20] Y. Sun, Y. Zhang, H.X. Zhang, M. Liu, Y. Liu, Integrating highly efficient recognition and signal transition of g-C3N4Embellished Ti3C2MXene hybrid nanosheets for electrogenerated chemiluminescence analysis of protein kinase activity, Anal. Chem. 92 (2020) 10668–10676, https://doi.org/10.1021/acs.analchem.0c01776.
[21] J. Low, B. Cheng, J. Yu, M. Jaroniec, Carbon-based two-dimensional layered materials for photocatalytic CO2 reduction to solar fuels, Energy Storage Mater. 3 (2016) 24–35, https://doi.org/10.1016/j.ensm.2015.12.003.
[22] A. Wang, C. Wang, L. Fu, W. Wong-Ng, Y. Lan, Recent advances of graphitic carbon nitride-based structures and applications in catalyst, sensing, imaging, and leds, Nano-Micro Lett. 9 (2017) 1–21, https://doi.org/10.1007/s40820-017-0148-2.
[23] M.M. Xavier, P.R. Nair, S. Mathew, Emerging trends in sensors based on carbon nitride materials, Analyst. 144 (2019) 1475–1491, https://doi.org/10.1039/c8an02110d.
[24] H. Liu, X. Wang, H. Wang, R. Nie, Synthesis and biomedical applications of graphitic carbon nitride quantum dots, J. Mater. Chem. B 7 (2019) 5432–5448, https://doi.org/10.1039/c9tb01410a.

[25] J.H. Thurston, N.M. Hunter, L.J. Wayment, K.A. Cornell, Urea-derived graphitic carbon nitride (u-g-C3N4) films with highly enhanced antimicrobial and sporicidal activity, J. Colloid Interface Sci. 505 (2017) 910–918, https://doi.org/10.1016/j.jcis.2017.06.089.
[26] G. Liao, F. He, Q. Li, L. Zhong, R. Zhao, H. Che, H. Gao, B. Fang, Emerging graphitic carbon nitride-based materials for biomedical applications, Prog. Mater. Sci. 112 (2020), https://doi.org/10.1016/j.pmatsci.2020.100666.
[27] T.Y. Ma, Y. Tang, S. Dai, S.Z. Qiao, Proton-functionalized two-dimensional graphitic carbon nitride nanosheet: An excellent metal-/label-free biosensing platform, Small. 10 (2014) 2382–2389, https://doi.org/10.1002/smll.201303827.
[28] M.H. Xiang, J.W. Liu, N. Li, H. Tang, R.Q. Yu, J.H. Jiang, A fluorescent graphitic carbon nitride nanosheet biosensor for highly sensitive, label-free detection of alkaline phosphatase, Nanoscale 8 (2016) 4727–4732, https://doi.org/10.1039/c5nr08278a.
[29] Z. Sun, H. Fu, L. Deng, J. Wang, Redox-active thionine-graphene oxide hybrid nanosheet: One-pot, rapid synthesis, and application as a sensing platform for uric acid, Anal. Chim. Acta 761 (2013) 84–91, https://doi.org/10.1016/j.aca.2012.11.057.
[30] C. Ou, R. Yuan, Y. Chai, M. Tang, R. Chai, X. He, A novel amperometric immunosensor based on layer-by-layer assembly of gold nanoparticles-multi-walled carbon nanotubes-thionine multilayer films on polyelectrolyte surface, Anal. Chim. Acta 603 (2007) 205–213, https://doi.org/10.1016/j.aca.2007.08.052.
[31] T. García-Mendiola, S. Requena-Sanz, E. Martínez-Periñán, I. Bravo, F. Pariente, E. Lorenzo, Influence of carbon nanodots on DNA-Thionine interaction. Application to breast cancer diagnosis, Electrochim. Acta 353 (2020), https://doi.org/10.1016/j.electacta.2020.136522.
[32] P. Kumar, D.K. Mahato, M. Kamle, T.K. Mohanta, S.G. Kang, Aflatoxins: A global concern for food safety, human health and their management, Front. Microbiol. 7 (2017), https://doi.org/10.3389/fmicb.2016.02170.
[33] K.R.N. Reddy, B. Salleh, B. Saad, H.K. Abbas, C.A. Abel, W.T. Shier, An overview of mycotoxin contamination in foods and its implications for human health, Toxin Rev. 29 (2010) 3–26, https://doi.org/10.3109/15569541003598553.
[34] S. Marchese, A. Polo, A. Ariano, S. Velotto, S. Costantini, L. Severino, Aflatoxin B1 and M1: Biological properties and their involvement in cancer development, Toxins 10 (2018), https://doi.org/10.3390/toxins10060214.
[35] Mycotoxins, (n.d.). https://www.who.int/news-room/fact-sheets/detail/mycotoxins (accessed October 26, 2020).
[36] Z. ben Abdallah, C. Grauby-Heywang, L. Beven, S. Cassagnere, F. Moroté, E. Maillard, H. Sghaier, T. Cohen Bouhacina, Development of an ultrasensitive label-free immunosensor for fungal aflatoxin B1 detection, Biochem. Eng. J. 150 (2019). https://doi.org/10.1016/j.bej.2019.107262
[37] S. Srivastava, V. Kumar, M.A. Ali, P.R. Solanki, A. Srivastava, G. Sumana, P.S. Saxena, A.G. Joshi, B.D. Malhotra, Electrophoretically deposited reduced graphene oxide platform for food toxin detection, Nanoscale 5 (2013) 3043–3051, https://doi.org/10.1039/c3nr32242d.
[38] M.P. Costa, I.A.M. Frías, C.A.S. Andrade, M.D.L. Oliveira, Impedimetric immunoassay for aflatoxin B1 using a cysteine modified gold electrode with covalently immobilized carbon nanotubes, Microchim. Acta 184 (2017) 3205–3213, https://doi.org/10.1007/s00604-017-2308-y.
[39] J. Xu, L. Zhang, R. Shi, Y. Zhu, Chemical exfoliation of graphitic carbon nitride for efficient heterogeneous photocatalysis, J. Mater. Chem. A 1 (2013) 14766–14772, https://doi.org/10.1039/c3ta13188b.
[40] Q. Cao, B. Kumru, M. Antonietti, B.V.K.J. Schmidt, Graphitic carbon nitride and polymers: A mutual combination for advanced properties, Mater. Horiz. 7 (2020) 762–786, https://doi.org/10.1039/c9mh01497g.
[41] C. Fan, J. Miao, G. Xu, J. Liu, J. Lv, Y. Wu, Graphitic carbon nitride nanosheets obtained by liquid stripping as efficient photocatalysts under visible light, RSC Adv. 7 (2017) 37185–37193, https://doi.org/10.1039/c7ra05732f.
[42] M. Davardoostmanesh, H. Ahmadzadeh, E.K. Goharshadi, A. Meshkini, E. Sistanipour, Graphitic carbon nitride nanosheets prepared by electrophoretic size fractionation as an anticancer agent against human bone carcinoma, Mater. Sci. Eng., C 111 (2020), https://doi.org/10.1016/j.msec.2020.110803.
[43] T. Jiang, G. Jiang, Q. Huang, H. Zhou, High-sensitive detection of dopamine using graphitic carbon nitride by electrochemical method, Mater. Res. Bull. 74 (2016) 271–277, https://doi.org/10.1016/j.materresbull.2015.10.049.
[44] Q. Zhuang, L. Sun, Y. Ni, One-step synthesis of graphitic carbon nitride nanosheets with the help of melamine and its application for fluorescence detection of mercuric ions, Talanta 164 (2017) 458–462, https://doi.org/10.1016/j.talanta.2016.12.004.
[45] W. Huang, A.K. Diallo, J.L. Dailey, K. Besar, H.E. Katz, Electrochemical processes and mechanistic aspects of field-effect sensors for biomolecules, J. Mater. Chem. C 3 (2015) 6445–6470, https://doi.org/10.1039/c5tc00755k.
[46] S. Kumar, S. Kumar, S. Tiwari, S. Augustine, S. Srivastava, B.K. Yadav, B.D. Malhotra, Highly sensitive protein functionalized nanostructured hafnium oxide based biosensing platform for non-invasive oral cancer detection, Sens. Actuators, B 235 (2016) 1–10, https://doi.org/10.1016/j.snb.2016.05.047.
[47] N. Elgrishi, K.J. Rountree, B.D. McCarthy, E.S. Rountree, T.T. Eisenhart, J.L. Dempsey, A practical beginner's guide to cyclic voltammetry, J. Chem. Educ. 95 (2018) 197–206, https://doi.org/10.1021/acs.jchemed.7b00361.
[48] C. Singh, S. Srivastava, M.A. Ali, T.K. Gupta, G. Sumana, A. Srivastava, R.B. Mathur, B.D. Malhotra, Carboxylated multiwalled carbon nanotubes based biosensor for aflatoxin detection, Sens. Actuators, B 185 (2013) 258–264, https://doi.org/10.1016/j.snb.2013.04.040.
[49] H. Bhardwaj, M.K. Pandey, G. Sumana Rajesh, Electrochemical Aflatoxin B1 immunosensor based on the use of graphene quantum dots and gold nanoparticles, Microchim. Acta 186 (2019), https://doi.org/10.1007/s00604-019-3701-5.
[50] K. Mahato, B. Purohit, K. Bhardwaj, A. Jaiswal, P. Chandra, Novel electrochemical biosensor for serotonin detection based on gold nanorattles decorated reduced graphene oxide in biological fluids and in vitro model, Biosens. Bioelectron. 142 (2019), https://doi.org/10.1016/j.bios.2019.111502.
[51] S. Srivastava, S. Abraham, C. Singh, A. Ali, A. Srivastava, G. Sumana, B.D. Malhotra, Protein conjugated carboxylated gold@reduced graphene oxide for aflatoxin B 1 detection, n.d. www.rsc.org/advances.
[52] H. Ma, J. Sun, Y. Zhang, S. Xia, Disposable amperometric immunosensor for simple and sensitive determination of aflatoxin B1 in wheat, Biochem. Eng. J. 115 (2016) 38–46, https://doi.org/10.1016/j.bej.2016.08.003.
[53] D. Zhou, M. Wang, J. Dong, S. Ai, A novel electrochemical immunosensor based on mesoporous graphitic carbon nitride for detection of subgroup j of avian leukosis viruses, Electrochim. Acta 205 (2016) 95–101, https://doi.org/10.1016/j.electacta.2016.04.101.
[54] A. Hatamie, P. Jalilian, E. Rezvani, A. Kakavand, A. Simchi, Fast and ultra-sensitive voltammetric detection of lead ions by two-dimensional graphitic carbon nitride (g-C3N4) nanolayers as glassy carbon electrode modifier, Measurement: J. Int. Meas. Confederation 134 (2019) 679–687, https://doi.org/10.1016/j.measurement.2018.10.082.
[55] J.H.O. Owino, O.A. Arotiba, N. Hendricks, E.A. Songa, N. Jahed, T.T. Waryo, R.F. Ngece, P.G.L. Baker, E.I. Iwuoha, Electrochemical immunosensor based on polythionine/gold nanoparticles for the determination of aflatoxin B1, Sensors 8 (2008) 8262–8274, https://doi.org/10.3390/s8128262.
[56] A. Sharma, Z. Matharu, G. Sumana, P.R. Solanki, C.G. Kim, B.D. Malhotra, Antibody immobilized cysteamine functionalized-gold nanoparticles for aflatoxin detection, Thin Solid Films (2010) 1213–1218, https://doi.org/10.1016/j.tsf.2010.08.071.
[57] A. Sharma, A. Kumar, R. Khan, Electrochemical immunosensor based on poly (3,4-ethylenedioxythiophene) modified with gold nanoparticle to detect aflatoxin B1, Mater. Sci. Eng., C 76 (2017) 802–809, https://doi.org/10.1016/j.msec.2017.03.146.
[58] X. Zhang, C.R. Li, W.C. Wang, J. Xue, Y.L. Huang, X.X. Yang, B. Tan, X.P. Zhou, C. Shao, S.J. Ding, J.F. Qiu, A novel electrochemical immunosensor for highly sensitive detection of aflatoxin B1 in corn using single-walled carbon nanotubes/chitosan, Food Chem. 192 (2016) 197–202, https://doi.org/10.1016/j.foodchem.2015.06.044.